AIAA 94-0711

Parallel Fuel Injection from the Base of an Extended Strut into Supersonic Flow

D.D. Glawe, J.M. Donbar, A.S. Nejad, B. Sekar
T.H. Chen (Taitech Group)
Aero Propulsion and Power Directorate
Wright-Patterson Air Force Base, OH

M. Samimy
Mechanical Engineering Department
The Ohio State University

J. F. Driscoll
Aerospace Engineering Department
University of Michigan

32nd Aerospace Sciences Meeting & Exhibit
January 10-13, 1994 / Reno, NV

Parallel Fuel Injection from the Base of an Extended Strut into Supersonic Flow

D.D. Glawe, J.M. Donbar, A.S. Nejad, B. Sekar
T.H. Chen (Taitech Group)
Aero Propulsion and Power Directorate
Wright-Patterson Air Force Base, OH 45433

M. Samimy
Mechanical Engineering Department
The Ohio State University, 43210

J. F. Driscoll
Aerospace Engineering Department
University of Michigan, 48109

Abstract

Planar Rayleigh/Mie scattering and acetone PLIF flow visualizations along with CFD results are presented for helium injected at sonic velocity into a nominal Mach 2 freestream air flow. The helium is injected parallel to the freestream from an extended strut with three different nozzle-to-freestream air static pressure ratios. Jet spread is insignificant for all three pressure cases. However, large scale, spatially periodic and organized structures are observed primarily in the under-expanded cases. The jet interaction is markedly three dimensional as exhibited by the irregular helium jet contour and the appearance of a conical shock in the highly under-expanded case. The Mach disk, jet spread, barrel shock and recirculation zone shown in the CFD results compare reasonably well to the planar Rayleigh/Mie scattering and the acetone PLIF images.

Introduction

Gaseous fuel injection into a supersonic airstream will be used in air-breathing hypersonic planes with supersonic combustion engines such as the National Aerospace Plane (NASP) and its derivatives. Several methods of injecting fuel into supersonic combustion ramjet (scramjet) engines have been proposed; among them is injection from a strut located in the upstream portion of the combustor.[1-3] This concept of strut injection leads to the experimental configuration outlined below. The engineering challenge for injection of fuel, either normal or parallel, into a supersonic freestream air flow is to produce optimal mixing with minimal losses within the space and time constraints of the combustor. Normal injection produces better mixing but causes major thrust losses primarily due to strong bow shocks.[4] Therefore, it would be advantageous to increase the extent of mixing in parallel injection to that of normal injection without incurring the associated thrust losses.

Passive means such as modified nozzle geometry,[5-9] selective initial conditions,[12] and acoustic excitation[13] have been shown to enhance mixing in subsonic parallel injection. However, injection and combustion in scramjets occurs at supersonic speeds (e.g., combustor Mach numbers of approximately 2 for flight Mach numbers of 7 or 8), and mixing characteristics are conceivably different under supersonic conditions compared to subsonic conditions. Although the effects of fluid compressibility encountered in supersonic flow can inhibit mixing,[14-17] shock waves can be generated to enhance mixing.[18-20] Continued studies through experiments and computational fluid dynamics (CFD) will cultivate a better understanding of mixing phenomenon in supersonic flows. The CFD results provide useful information for the design of experiments and the experimental results provide a detailed data base for future CFD work and to gage the accuracy of the CFD results.

The objective of this research is to investigate supersonic parallel injection and mixing through observation and measurements of flow parameters using acetone Planar Laser Induced Fluorescence (PLIF), planar Rayleigh/Mie scattering, and comparison to CFD results. The first consideration in this research is the injection model. The injection nozzle needs to be mounted inside the supersonic tunnel with minimal upstream disturbances to eliminate extraneous factors from the experiments. A strut provides rigid support for the nozzles and the added benefit of a recirculation zone for flame holding in combustion applications. This strut is similar to a typical splitter plate used in shear layer studies except that the flow velocity is the same on both sides of the strut and the base of the strut is blunt rather than tapered to a knife edge. By extending the strut upstream through the nozzle into the settling chamber and using the method of characteristics to design the nozzles, shock waves are eliminated in the free stream before reaching the end of the strut. Although the strut and injection nozzle are of a simple geometry, the two-dimensional expansion of the freestream over the base, combined with the axisymmetry of the jet result

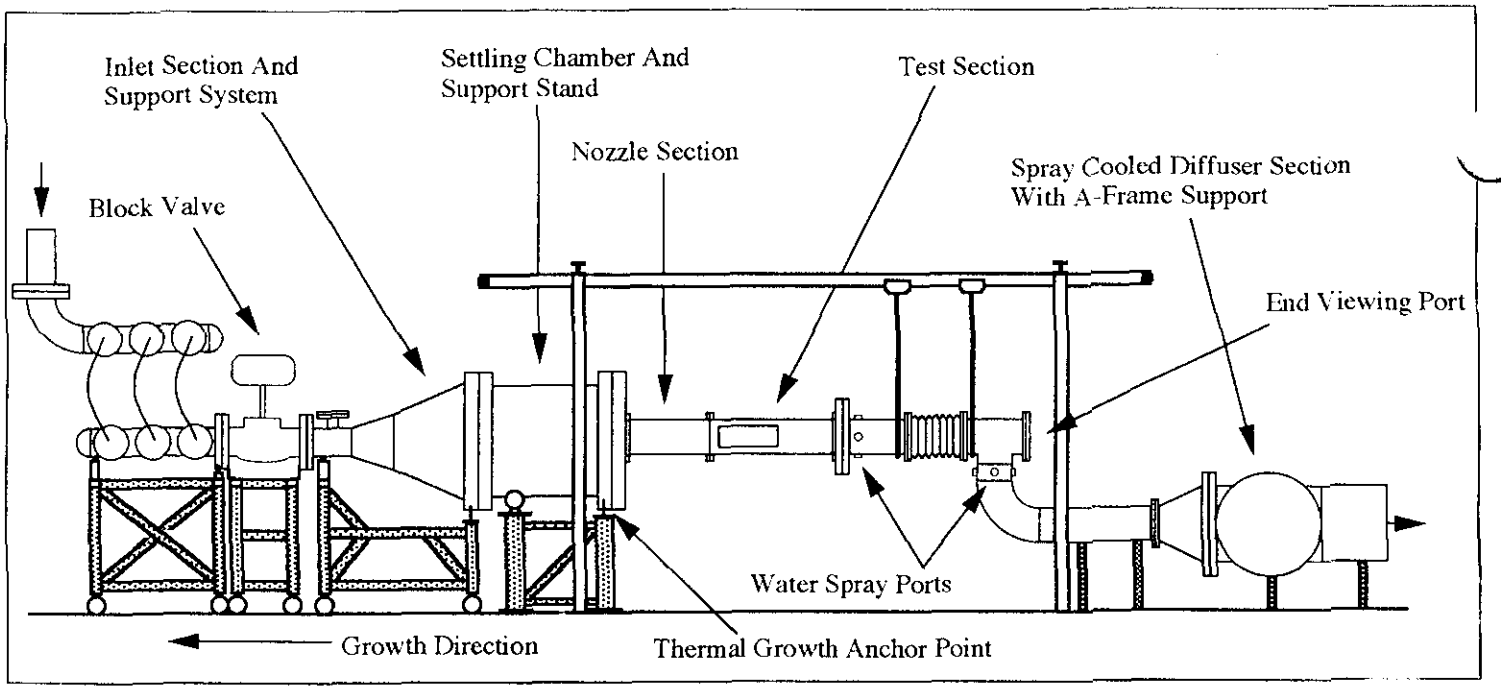

Figure 1 Schematic of supersonic combustion tunnel

in a complex three-dimensional flow field. The flow characteristics of this design are intermediate between two-dimensional slot injection from a base and parallel injection from an axisymmetric configuration.

Experimental Facility

This research was conducted in the newly built supersonic combustion research facility at the Aero Propulsion and Power Directorate, Wright Patterson Air Force Base.[21] The wind tunnel is capable of continuous flow operation at maximum stagnation conditions of 400 psia (2.75 MPa) and 1660 R (889 K) at a peak flow rate of 34 lbm/s (15.5 kg/s) with the test section design static condition being 7.35 psia (51 KPa) and 525 R (292 K). The test section temperature and pressure conditions are adjusted by mixing air from hot and cold supply lines in controlled quantities. The nominal 5 by 6 in. (12.70 x 15.24 cm) test section has optical access from three sides and from the downstream end. A tunnel schematic is shown in Figure 1.

The 0.5 in. (1.27 cm) thick strut extends from the settling chamber, through the nozzle section and into the test section, thus avoiding leading edge shock waves. The Mach 2 nozzle (Figure 2) was designed by the method of characteristics to eliminate shock waves and provide a uniform, nominal Mach 2.0 freestream flow before reaching the end of the extended strut where injection occurs. The plumbing for the injector runs through the sidewall of the tunnel into the strut and is directed through a 90 degree bend to enter a circular converging nozzle. The nozzle is inserted into the center of the trailing end of the strut. The nozzle is directly preceded by a straight section that is over 40 injector diameters in length. Helium is used as the injectant to simulate hydrogen which will be used in future hydrogen/air combustion tests. Helium exits at sonic velocity from a 0.138 in. (3.5 mm) diameter converging circular nozzle (Figure 2).

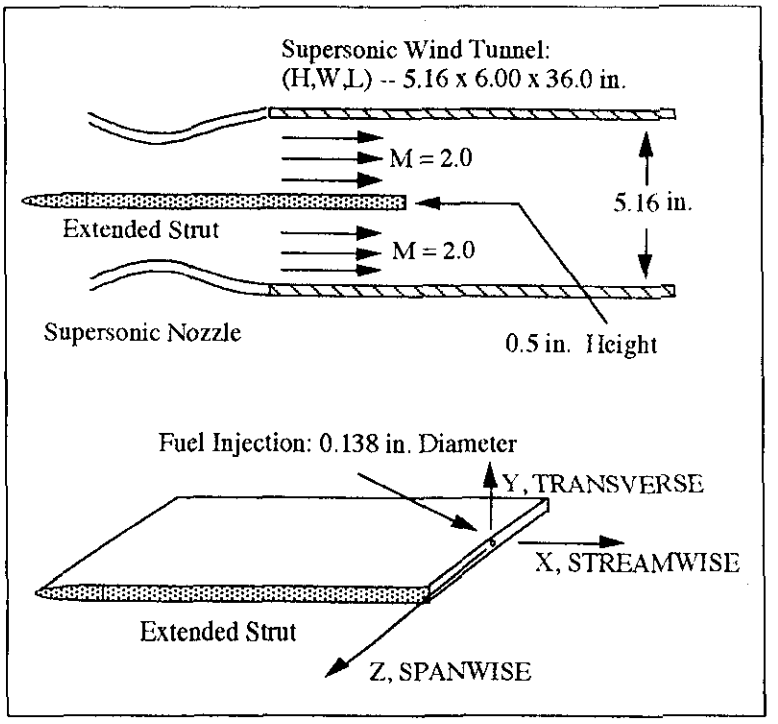

Figure 2 Schematic of extended strut and reference coordinate system

Flow Diagnostics

Planar Rayleigh/Mie Scattering

A Lambda Physik EMG 150 Excimer laser produced the 248 nm wavelength ultra-violet radiation used for Rayleigh/Mie scattering. The laser beam was transformed into a sheet, approximately 0.5 mm thick, and projected through the test section by a series of lenses and prisms as shown in Figure 3. A Princeton Instrument Intensified Charge Coupled Device (ICCD) camera with forced cooling captured images of the flow on command and stored them in a central processing unit (CPU) for subsequent analysis. The signal was collected through a Nikon UV-Nikkor 105 mm f/4.5 telephoto lens and was imaged onto the 578 by 384 pixel array of the ICCD camera. The effective gate width of approximately 10 ns, which is the laser temporal pulse width, is sufficiently short in duration to consider the images instantaneous. To keep the plane of interrogation in focus, the ICCD camera was mounted on the same three axis transversing table as the optics so that the laser sheet and camera moved in unison.

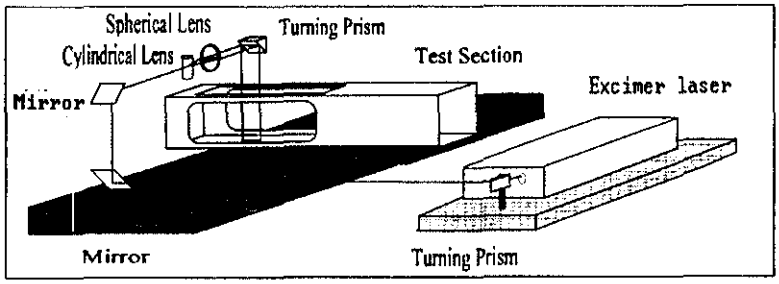

Figure 3 Mie scattering optical arrangement

Naturally occurring moisture in the wind tunnel condenses to form an ice "fog" that effectively scatters the UV radiation. The resulting scattering highlights shock waves in the freestream and the mixing of the freestream air with the injected helium jet. Figure 4 a,b,c are schematic representations of the flow field as seen using the planar Rayleigh/Mie scattering technique. They are provided to outline the features of the flow field for reference when viewing the actual Rayleigh/Mie images. This visualization method with naturally occurring moisture has previously been used in supersonic boundary layers[22,23] and mixing layers.[24] Likewise, condensed droplets of ethanol added to the freestream flow have previously been used in visualizing supersonic mixing layers[25] and a transverse sonic jet.[26,27] However, these particles are not conserved scalars throughout the flow since the fluid temperature changes as it passes through shock waves, expansion waves, and viscosity dominated regions (i.e., boundary layer), possibly creating or destroying particles by condensation and evaporation respectively. A change in scattered light due to temperature change (particles being created/destroyed) cannot be discerned from an increase/decrease in scattered light due to existing particles amassing in a particular region.

The information contained in these images is analogous whether the scattering is Rayleigh or Mie. As long as the particles follow the flow, their size is not of critical importance. Because the particles are formed through a homogeneous nucleation process,[25] they are probably small. Evaluation of particle size by Elliot[24] in nominal Mach 2 and 3 freestream showed the particles to scatter light in the

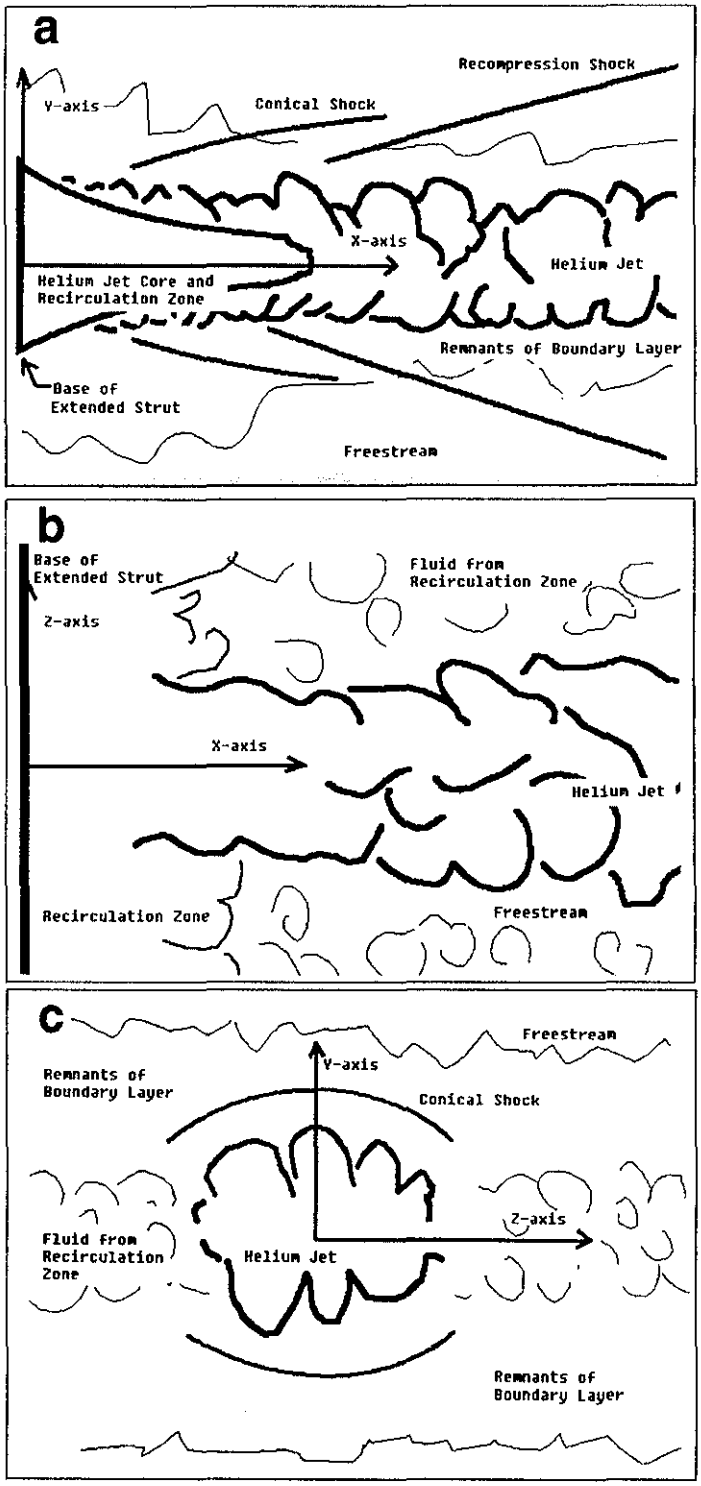

Figure 4 Schematic of planar Rayleigh/Mie images
a) streamwise b) planar and c) face-on views

Rayleigh regime for a wavelength of 532 nm. The particles of the present study seem to follow the flow as represented by ligaments of freestream fluid, which contains particles, entrained in the helium Jet (discussed in the Results portion of this paper). Future work will include measurements of the particle size.

Acetone PLIF

A frequency doubled Spectra-Physics Quanta-Ray DCR-4 Nd:YAG laser (532 nm wavelength beam) in conjunction with a Quanta-Ray wavelength extender (WEX-1) produced the ultra-violet radiation (266 nm) for acetone PLIF. The acetone added to the helium jet was regulated and metered along with the helium gas flow rate. The same optical system as shown in Figure 3 was used except that the Excimer laser was replaced by the YAG/WEX system. Likewise, the same imaging system was used as in the Rayleigh/Mie set-up except that a Nikon Nikkor 60 mm f/2.8 Micro lens replaced the UV telephoto lens. Because of the visible fluorescence, an ordinary camera lens can be used; an added advantage of an ordinary lens is that it effectively blocks the strong particle scattering at 266 nm.

The acetone PLIF images show the internal shock structure of the injected helium jet (see the schematic in Figure 5). Acetone has proven to be superior to other molecular tracers because of its high signal to noise ratio, non-toxic nature, and an excitation frequency that is easily accessible by different lasers.[28] Acetone (CH3-CO-CH3) has a molecular weight of 58.08, a specific gravity of 0.79, and a vapor pressure of 3.48 psia (24 KPa) at 527 R (293 K). It absorbs light and is excited from a ground singlet state to a first excited singlet state in the 225-320 nm wavelength band. Most of the excited acetone molecules in the singlet state are transferred to the triplet state and almost all of the remaining excited singlet molecules fluoresce in the 350-600 nm wavelength band with a lifetime of a few nanoseconds. The triplet state molecules undergo phosphorescence which is shifted toward the red with respect to the singlet-state fluorescence, with a natural lifetime of approximately 200 μs.[29,30] However, the triplet state is effectively quenched by O_2. The limited gate width of the camera captures only the fluorescence signal. The aforementioned acetone characteristics are included in a more detailed description by Lozano et al.[28]

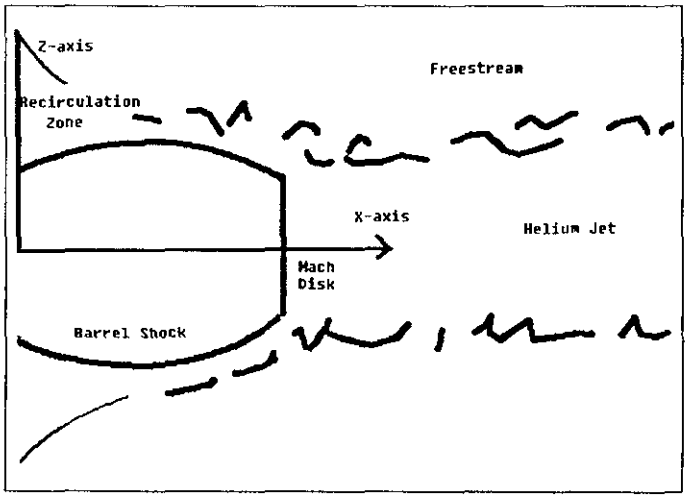

Figure 5 Schematic of PLIF image, streamwise view

CFD Code and Conditions

All numerical results presented here were obtained through the use of the General Aerodynamic Simulation Program (GASP). All numerical results are three-dimensional and include the combustion tunnel nozzle solution starting from the subsonic portion of the nozzle, the throat area, subsequent expansion in the supersonic portion in the nozzle and the mixing regions starting at the base of the extended strut. All results were obtained using the flux-differencing scheme of Roe. In addition, Sutherland's law is used to determine individual laminar species viscosity while Wilke's rule is used to determine the mixture viscosity. The Baldwin-Lomax eddy viscosity model accounts for turbulence. Perfect gases are assumed and binary diffusion can occur under the presence of mass fraction gradients. The binary diffusion coefficient is calculated using a constant Schmidt number of 0.5.[31] Air and helium input conditions for the code were chosen to match

Table 1 Operating conditions for helium injection into Mach 2 air freestream

	Po	To	Mach #	P∞	t∞	ρ∞	u∞
	Pa	K		Pa	K	kg/m^3	m/s
Freestream	295,442	300	2.0	37,758	167	0.7894	518
He Case 1x	92,755	339	1.0	45,181	254	0.8556	939
He Case 2x	164,898	339	1.0	80,322	254	0.1521	939
He Case 4x	398,503	339	1.0	194,111	254	0.3676	939

the experimental operating conditions listed in Table 1.

The calculations were carried out in a multi-zone fashion with two zones in the nozzle region, one upstream of the base edge of the strut and two downstream of the injection point. For the two mixing zones, complete Reynolds averaged Navier-Stokes equations are solved. Locally, 3rd order computations of inviscid flux contributions in the streamwise and transverse directions are used in conjunction with 1st order accurate contributions of inviscid terms in the spanwise direction. Viscous contributions are second order accurate. Wall boundaries are treated as adiabatic, and first order computation of gradients at the wall are used.

Due to symmetry, only one quarter of the injector configuration was modeled. The near field around the injector is an unsteady and complex flow field. The goal of the CFD investigation was to capture the bulk characteristics of the mean flow to compliment the instantaneous experimental images. Note that the individual instantaneous experimental images are representative of the relevant time-averaged experimental images of the flowfield, thus making direct comparison between CFD and experimental results meaningful.

Results and Discussion

The helium is injected at nozzle-to-freestream air static pressure ratios of 1, 2, and 4 (denoted as cases 1x, 2x and 4x); these operating conditions are summarized in Table 1. Figure 4 shows schematic drawings of the three orthoganol planes of view for the Rayleigh/ Mie scattering technique: streamwise, planar, and face-on. Both the streamwise and the planar images represent a 1.7 by 1.1 in. field of view, with the flow direction being left to right. With the 578 by 384 pixel array of the camera, this corresponds to an apparent resolution of 0.0030 in. (76.2 m) per pixel. However, the overall resolution is limited by the laser sheet thickness of about 0.5 mm. The face-on view has a 1.2 by 0.8 in.

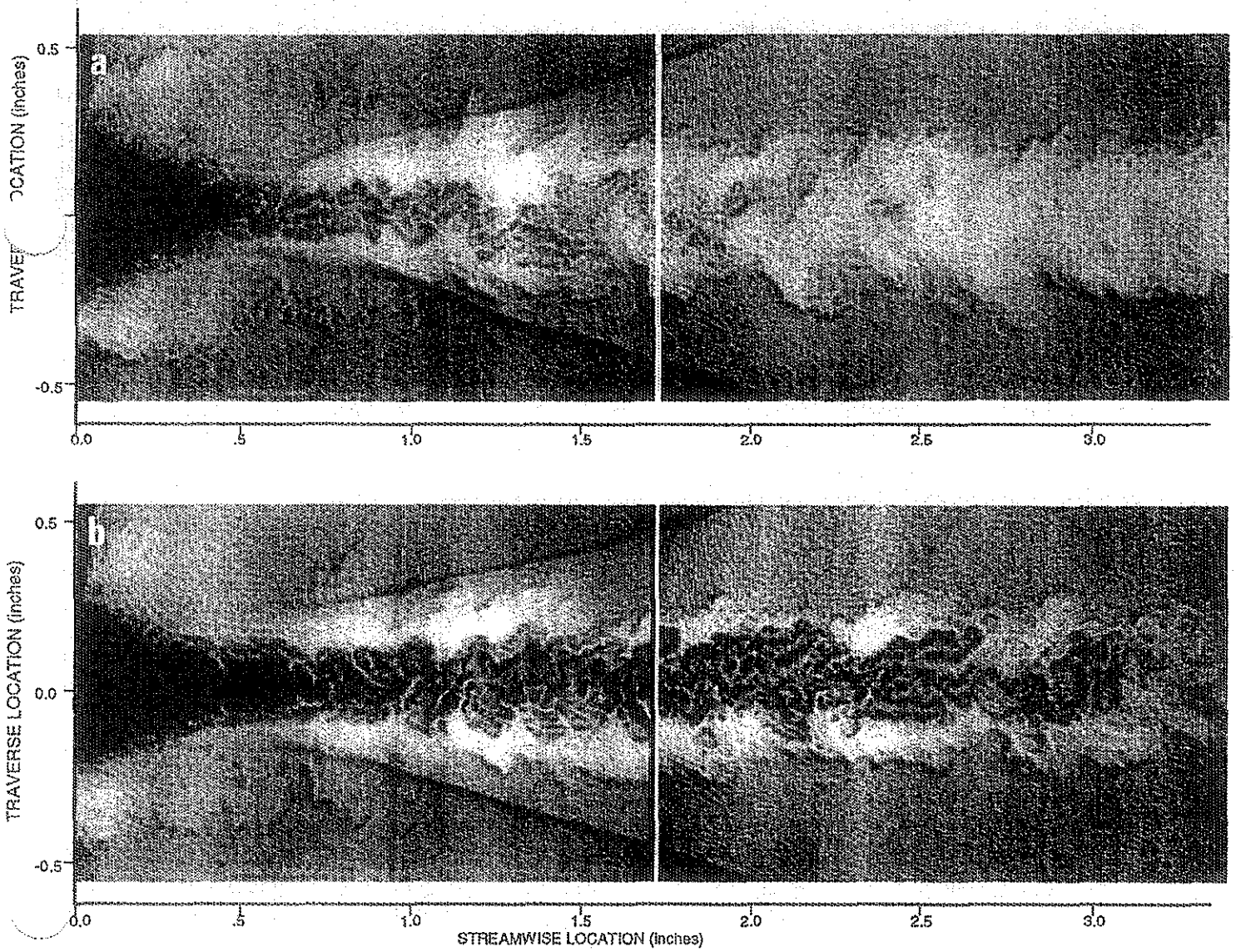

Figure 6 Streamwise views on centerline of a) no-injection and b) 1x pressure matched cases

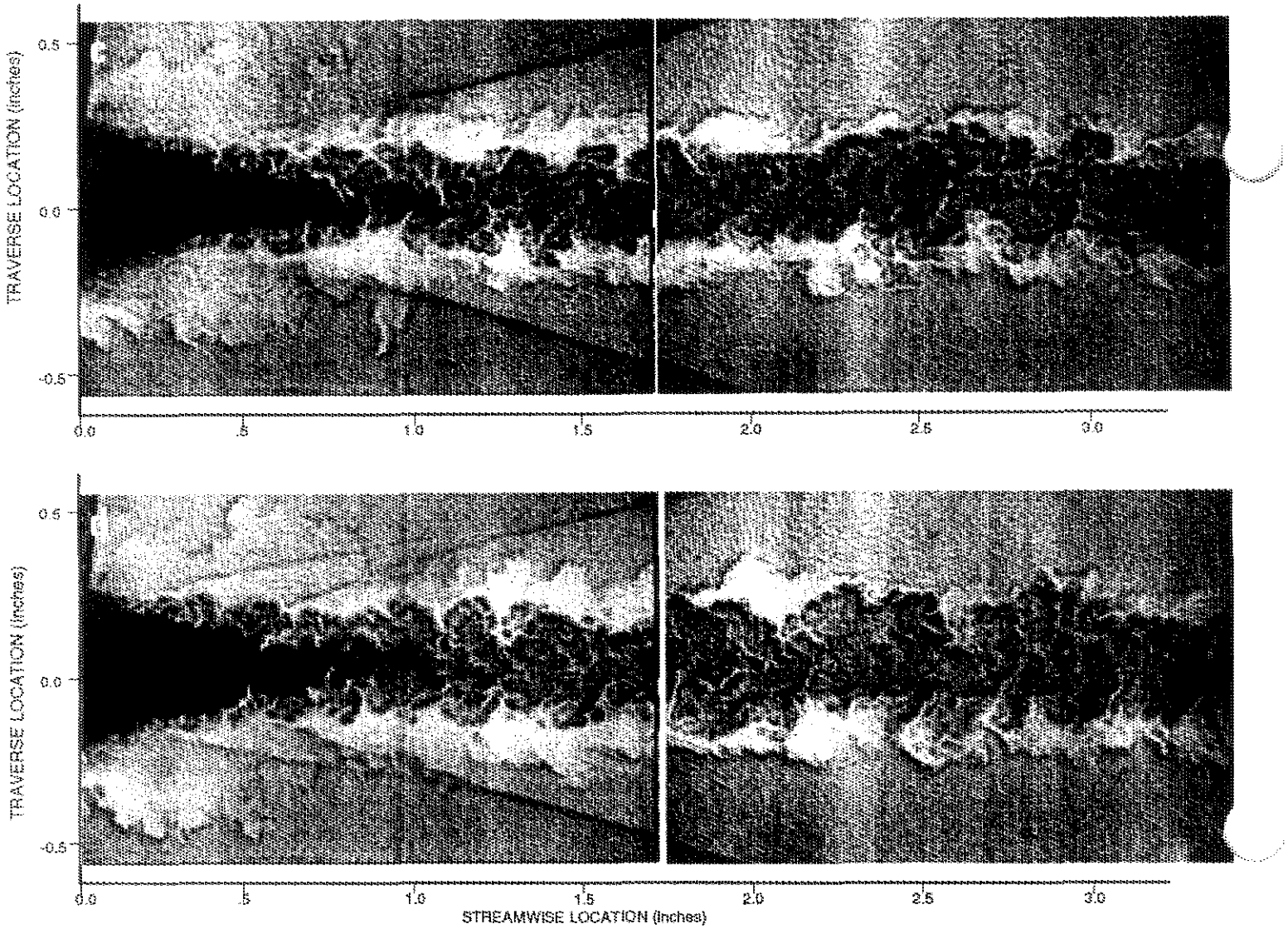

Figure 6 Streamwise views on centerline of c) 2x and d) 4x pressure matched cases

field of view with the flow direction being out of the plane of the page. Figure 5 shows the schematic drawing for the streamwise view for acetone PLIF, which has a 0.80 by 0.53 in. field of view.

Figure 6 shows Mie scattering images for all four cases studied: no injection, 1x, 2x, and 4x. This figure includes upstream and downstream views (taken during different laser pulses), separated by a white line, for each pressure condition. The images are not corrected for laser intensity variation or background, but the contrast is adjusted for print quality. The jet does not penetrate transversely beyond the strut 'boundary layer remnants' (i.e., fluid downstream of the strut base that was initially in the boundary layer), except for some structures in the 2x and 4x cases. The 'boundary layer remnants' are identified in the images as the most intense region of the freestream that borders the helium jet (Figures 4 and 6). This is similar to observations made in a comparable normal injection case where these 'boundary layer remnants' appear to 'ride' atop the injectant fluid.[37]

The field of view presented is limited to 25 jet diameters downstream of injection. Jet behavior may differ further downstream. The temperature and pressure of the 'boundary layer remnants' change with passage through the expansion fan and shock wave(s). This may decrease/increase the scattering signal intensity as previously discussed. The images show the boundary layer to be approximately 0.17 in. (4.3 mm) thick before reaching the base of the extended strut, while CFD results predict a 0.13 in. (3.3 mm) thick boundary layer.

From the streamwise views similar to Figure 6, average jet core lengths and recompression shock angles can be estimated. Conventional definitions of the jet core are based on injectant gas concentration measurements. Since the intensity change is not a known function of concentration in these images, determination of the core length is an approximation. The recirculation zone for the no injection case was observed to extend approximately 0.40 in. beyond the base of the strut in the direction of flow. The 0.40 in.

length of the recirculation zone relative to the 0.50 in. strut width is similar to observations in subsonic flow.[33] The recirculation/jet-core zone extends about 0.25 to 0.35 in. beyond this in all three injection cases. The recompression shock angles remain about the same for all three injection pressures and the no injection case. The slight variation between 12 and 16 degrees, measured with respect to the streamwise axis, indicates that the near-field injection plume does not significantly alter the freestream recompression shock angle. The large density and pressure gradients associated with the recompression shock are difficult to locate precisely in the CFD results because of the limited resolution of the three-dimensional CFD generation grid. However, the CFD results do show an increase in density and pressure across a region surrounding the presumed location of the recompression shock.

Figure 7 shows corresponding face-on Rayleigh/Mie images and CFD results for the 1x and 4x cases at a streamwise location of 0.5 in. (1.27 cm). Note that the face-on spanwise images are elongated along the spanwise axis due to a 27 degree angle between the camera axis and the flow axis. After calculating trigonometric corrections for this distortion, the jet contour is still oblong with the major axis along the spanwise axis. The eccentricity ($\varepsilon = \sqrt{1 - b^2/a^2}$ where a,b are the semi-major and semi-minor axes, respectively) of the jet core region is greater than 0.86 for all injection cases.

The large scale mixing with the freestream fluid occurs primarily in the transverse direction as illustrated by the 'lobed' structures along the periphery of the jet contour in the transverse direction. These lobes are most visible in the 4x case (Figure 7b), but can be seen in the 2x and 1x cases (Figure 7a) as well. For the under-expanded cases where the structures are distinctly visible, the structures appear in the same position on the 5 images recorded at each location. Therefore, a time averaged image, corresponding to the CFD results, would show structures similar to those on the instantaneous images. The corresponding CFD plots of helium mole fraction (Figures 7c,d) show protuberances similar in appearance to the lobed

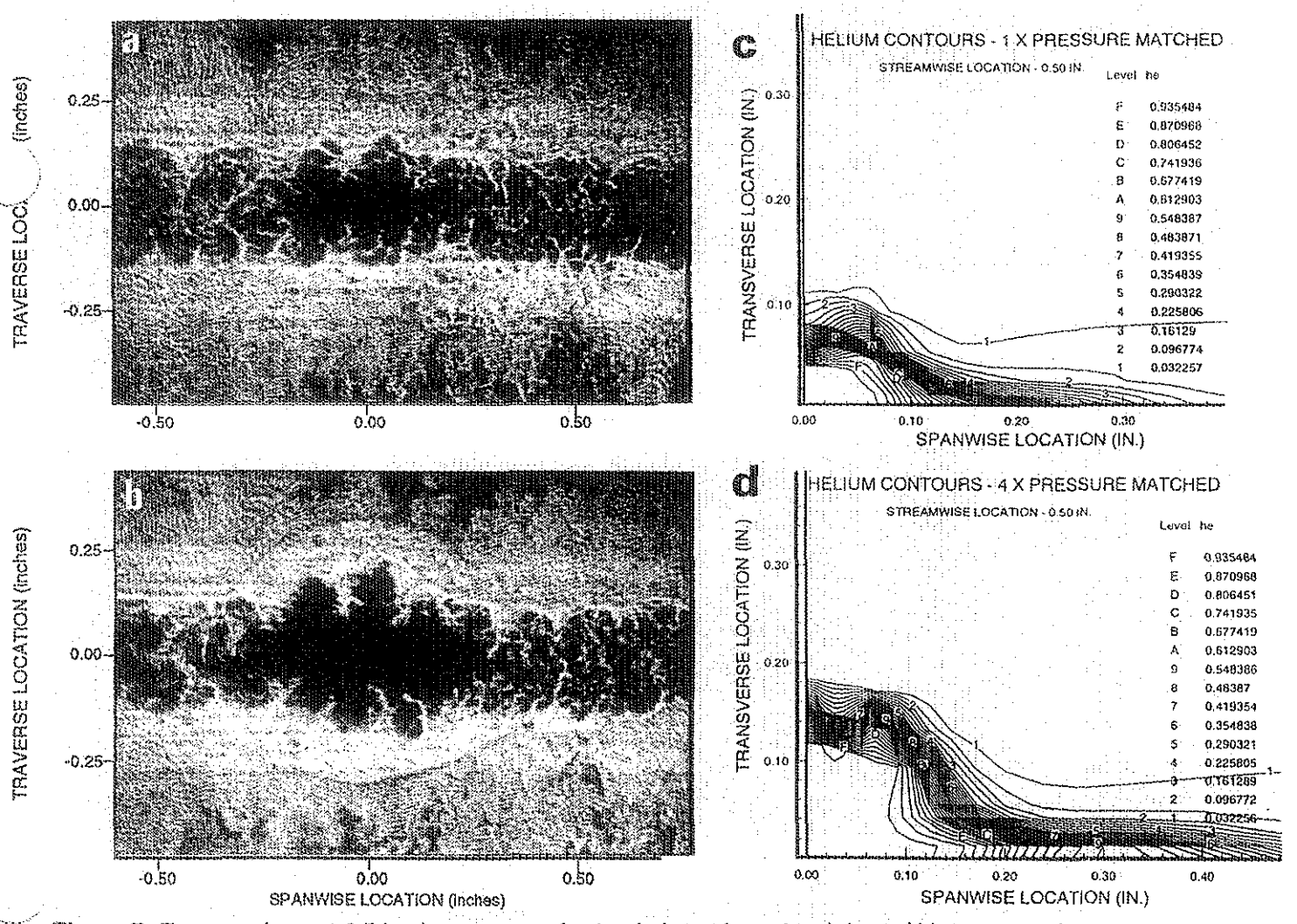

Figure 7 Face-on views at 0.5 in. downstream of extended strut base for a) 1x and b) 4x case using Rayleigh/Mie scattering and c) 1x d) 4x pressure matched case using results of CFD

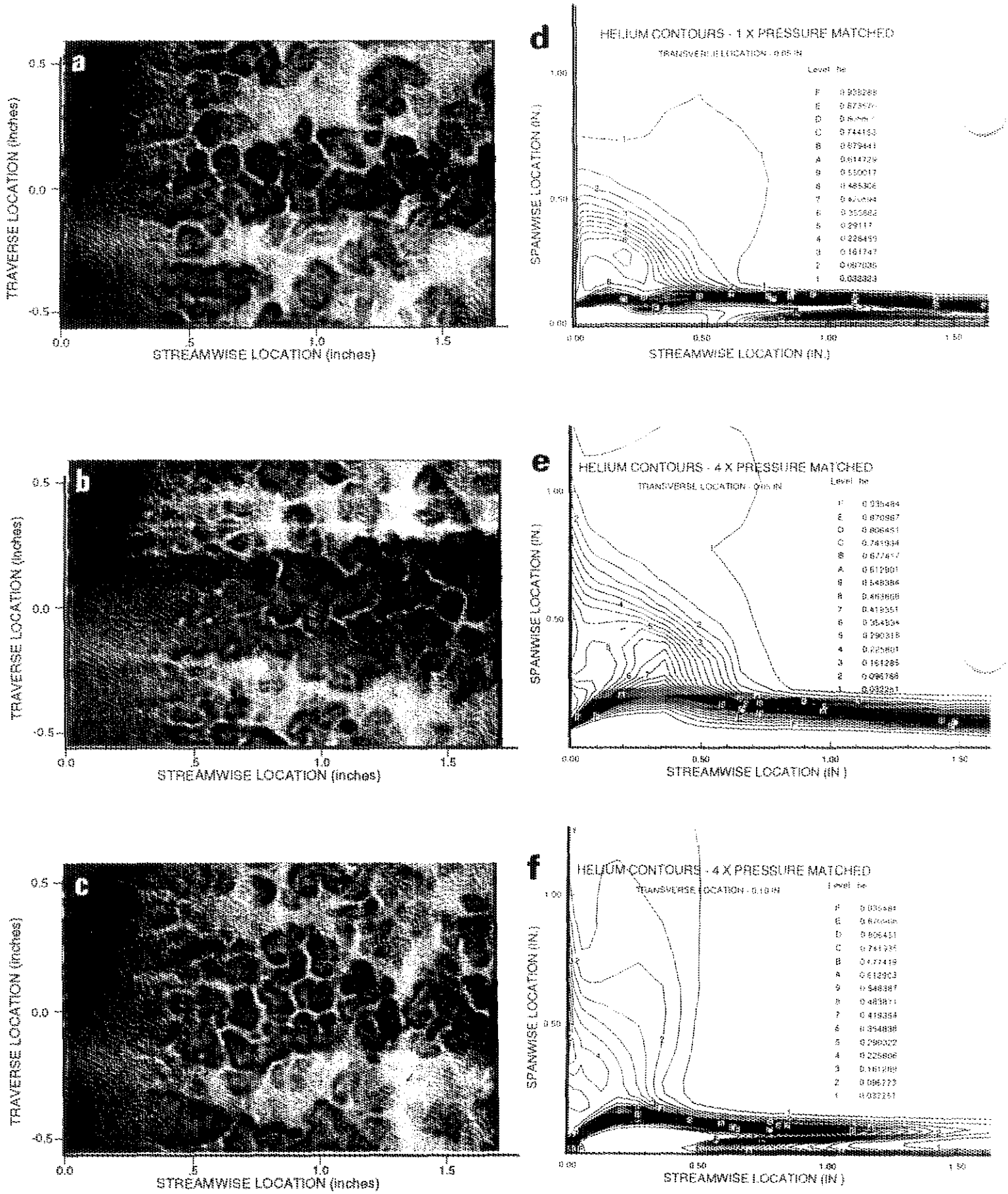

Figure 8 Planar views for a) 1x and b) 4x cases at 0.05 in. off centerline and c) 4x case at 0.10 in. off centerline in the transverse direction using Rayleigh/Mie scattering the corresponding helium concentration profiles are shown in plots d, e, and f.

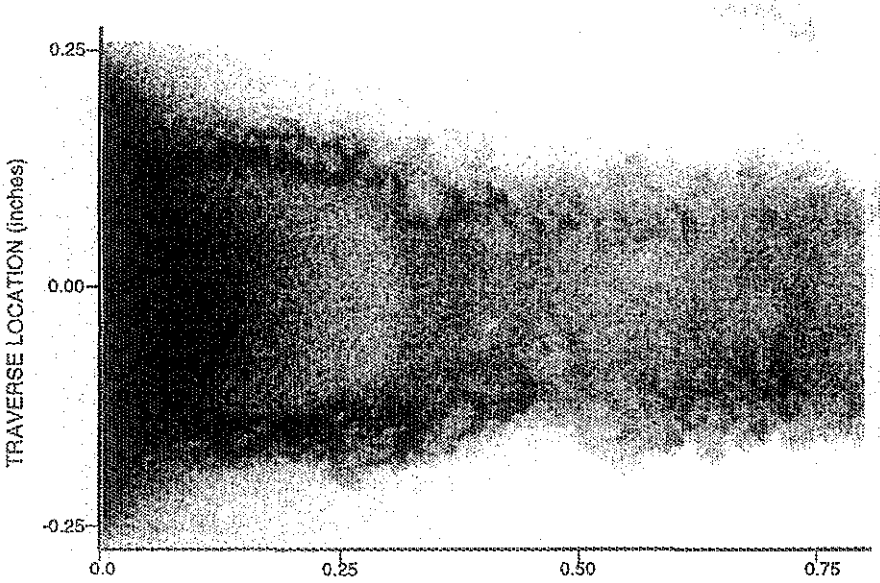

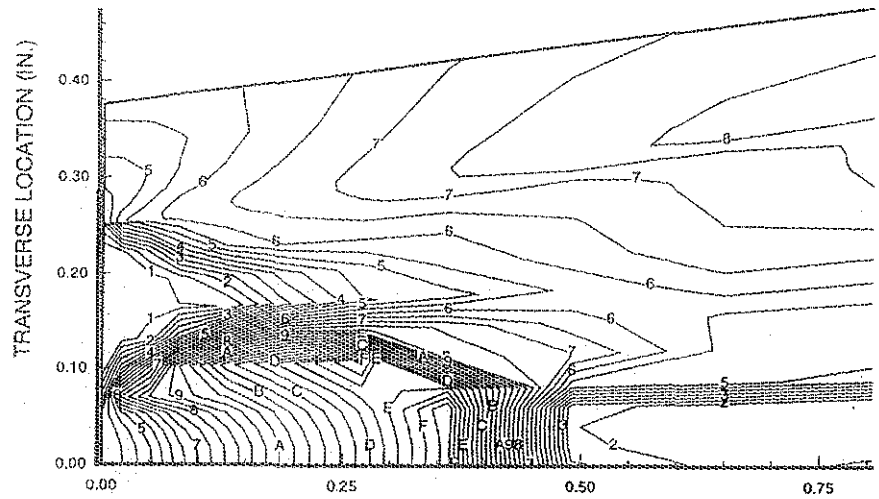

Level M

F	4.95652
E	4.61504
D	4.27356
C	3.93209
B	3.59061
A	3.24913
9	2.90765
8	2.56617
7	2.2247
6	1.88322
5	1.54174
4	1.20026
3	0.858782
2	0.517304
1	0.175826

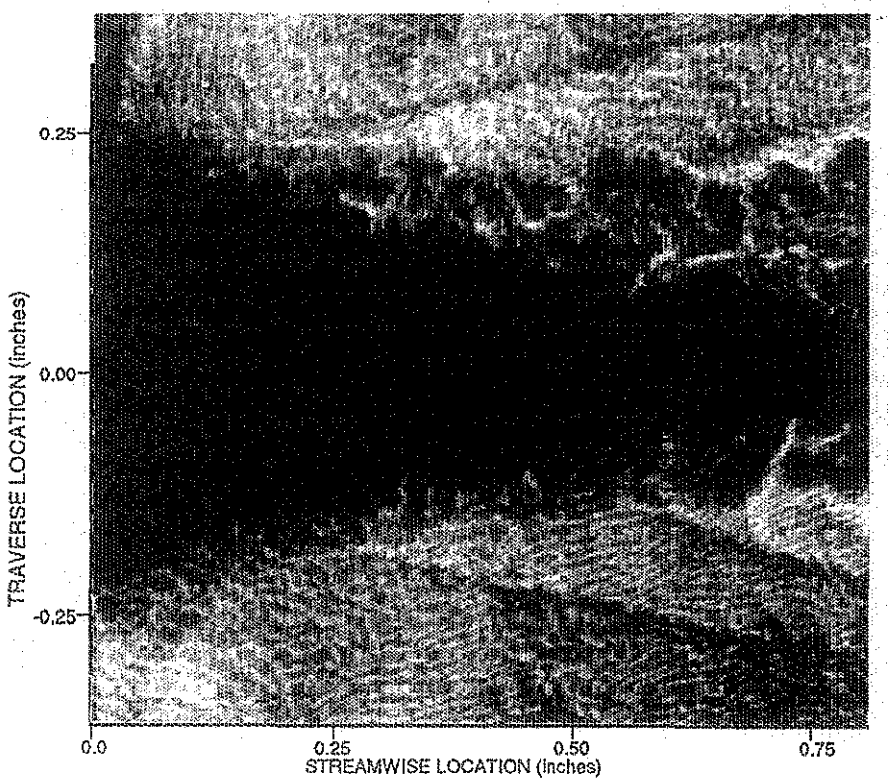

Figure 9
Streamwise views on centerline for 4x pressure matched case:
a) Acetone PLIF
b) CFD generated Mach contours
c) Planar Rayleigh/Mie scattering

structures. Note that the CFD scale is more than twice the size of the image scale for better visibility of the protuberances.

Images taken in the other two orthoganol planes of view show these large scaled structures as well. Figure 8a,b shows planar cut images at a transverse location 0.05 in. (1.27 mm) above the centerline for the 1x and 4x cases. This view reveals consecutive sets of helium lobes propagating downstream (dark regions) and the entrained freestream fluid layer between them (bright ligaments). The lobes in the 4x case are not as distinct as the 1x case at this transverse location. The corresponding CFD plots (Figure 8d,e) of helium concentration show similar results. The CFD plot for the 1x case shows noticeable spacial fluctuations of helium concentration across the jet, whereas the plot of the 4x case is more uniform. This concentration difference corresponds to the appearance of more distinct bright freestream ligaments in the image of the 1x case. However a planar cut at 0.10 in. (2.54 mm) above the centerline for the 4x pressure case (Figure 8e) shows the same type of separation between structures as the 1x case at 0.05 in. This indicates that structures reach further in the transverse direction for the 4x case. Comparison of the corresponding CFD images (Figure 8d,f) supports the above observation.

Figure 9 displays close-up, streamwise views using PLIF, CFD, and Rayleigh/Mie data for the region immediately downstream of the injector for the 4x case. Upon leaving the injector, the under-expanded helium continues to accelerate until a barrel shock/Mach disk mechanism acts to raise the pressure to the required freestream value. This acceleration is captured in the PLIF images as a significant decrease in signal intensity (Figure 9a). The CFD results (Figure 9b) predict the location of the Mach disk reasonably well by comparison to the PLIF images, and estimate the final expansion Mach number to be approximately 5 for the 4x case. Similar results for the 1x and 2x cases indicate final expansion Mach numbers of 3.5 and 4, respectively. It is believed that the bending of the freestream fluid as it flows off the end of the extended strut and encounters the side region of the barrel shock causes a second shock to appear upstream of the recompression shock (Figure 9c). This shock also appears as a shadow-like outline of a bright ellipse surrounding the helium jet in the face-on view (Figure 7b). Comparing these two views reveals that the shock wave is cone shaped. This conical shock, however, does not appear in the 1x or 2x cases. One possible explanation is that the conical shock coalesces with the recompression shock in the 2x case. Another more likely explanation is that the influence of the barrel shock for the 2x case does not extend beyond the buffer region of the recirculation zone. The 1x case is pressure matched and has no barrel shock.

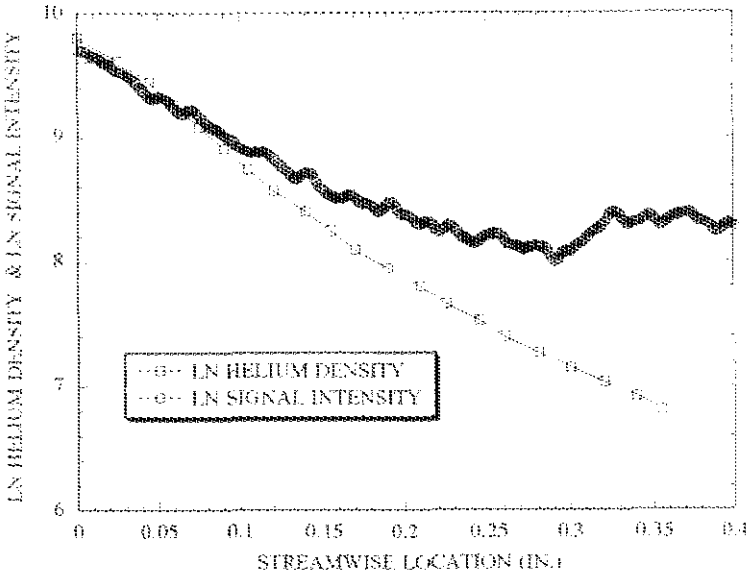

Figure 10 Natural log (LN) of helium density compared to natural log of signal intensity

The use of acetone for injectant concentration measurements, as demonstrated in Figure 9a, is promising. However, the lack of signal intensity inside the barrel shock, where the helium and air have not yet mixed, indicates the signal intensity is not solely a function of mixture fraction. Instead, the fluorescence intensity apparently follows the helium number density. This behavior is expected when the spontaneous emission rate is much greater than the quenching rate.[29] Figure 10 shows a logarithmic plot comparing collected signal intensity to CFD calculated helium density for the near field region of Figure 10. The curves agree in the extreme near field but begin to diverge further downstream. This difference may be due to several factors which include, but are not limited to, laser sheet variations, the effects of unidentified flow phenomena on the fluorescence signal, and possible CFD inaccuracies. Until further studies have been completed and this relationship is completely understood, direct mixture fraction measurements from the PLIF signal are not possible.

Conclusions

The sonic helium jet that was injected coaxially into a Mach 2 airstream did not spread significantly for any of the three pressure cases considered. The jet fluid remains within the remnants of the splitter plate boundary layer with the exception of some large scale structures reaching into the freestream (particularly for the 4x case). However, the jet does spread predominantly along the spanwise direction creating an oblong jet contour with large scale structures evident along the transverse axis of the jet. These structures appear to be spatially periodic and more organized in the under-expanded cases as compared to the pressure matched case. The jet spread is markedly three-dimensional as

seen by the irregular jet contours downstream of injection and by the conical shock in the highly under-expanded case.

The numerical simulation captures the essential features of the flow field, namely the barrel shock, Mach disk, recirculation region, and expansion zone. In addition, the Mach disk location and helium jet spread predicted by these numerical simulations agree reasonably well with the Rayleigh/Mie scattering and acetone PLIF images from experiments.

Future studies will involve other appropriate measurement techniques and mixing enhancement schemes. Laser Doppler Velocimetry (LDV) measurements will allow more precise determination of the jet width and the boundary layer thickness in addition to providing statistical velocity information. Acetone PLIF, with refinement, will provide more detailed information about the extent of mixing. Passive mixing enhancement by the use of different nozzle geometries and stationary impinging shock waves will be explored. When concentration and velocity information become available, the GASP code will be tested further.

Acknowledgements

The support of Dr. Julian Tishkoff and the Air Force Office of Scientific Research is greatly appreciated. Special thanks to Dave Schommer, Charles Smith, and Campbell Carter for their technical assistance.

References

[1]Jacobs, P.A., Rogers, R.C., Weidner, E.H., and Bittner, R.D., "Flow Establishment in a Generic Scramjet Combustor," AIAA Paper 90-2096, 1990.

[2]Northam, G.B., Trexler, C.A., and McClinton, C., "Flameholding Characteristics of a Swept Strut Hydrogen Fuel Injector for Scramjet Application," NASA TR A81-10711, 1981.

[3]Anderson, G.Y., Reagon, P.G. Gooderum, P.B., and Russin, W.R., "Experimental Investigation of a Swept Strut Fuel Injector concept for Scramjet Application," NASA TN D-8454, 1977.

[4]King, P.S., Thomas, R.H., Schetz, J.A., Billig, F.S., "Combined Tangential-Normal Injection Into a Supersonic Flow," AIAA Paper 89-0622, 1989.

[5]Ho,C.M., and Gutmark, E., "Vortex Induction and Mass Entrainment in a Small-Aspect-Ratio Elliptic Jet," *J. Fluid Mech.*, Vol. 179, 1987, pp. 383-405.

[6]Gutmark, E., Schadow, K.C., and Wilson, K.J., "Subsonic and Supersonic Combustion Using Non-Axisymmetric Injectors," AIAA Paper 88-3141, 1988.

[7]Gutmark, E., Schadow, K.C., and Wilson, K.J.,"Noncircular Jet Dynamics in Supersonic Combustion," *J. Propulsion*, Vol. 5, No. 5, 1989, pp. 529-533.

[8]Quinn, W.R., "On Mixing in an Elliptic Turbulent Free Jet," *Phys. Fluids A*, Vol. 1, No. 10, 1989, pp. 1716-1722.

[9]Samimy, M., Zaman, K.B.M.Q., and Reeder, M.F., "Effect of Tabs on the Flow and Noise Field of an Axisymmetric Jet," *AIAA Journal*, Vol. 31, No. 4, 1993, pp. 609-619.

[10]Wlezien, R.W., and Kibens, V., "Influence of Nozzle Asymmetry on Supersonic Jets," *AIAA Journal*, Jan. 1988, pp. 27-33.

[11]Longmire, E.K., Eaton, J.K., and Elkins, C.J., "Control of Jet Structure by Crown-Shaped Nozzles," *AIAA J.*, Vol. 30, No. 2, 1992, pp. 505-512.

[12]Hussain, A,K.M.F., and Zedan, M.F., "Effects of the Initial Condition of the Axisymmetric Free Shear Layer: Effects of the Initial Momentum Thickness," *Phys. Fluids*, Vol. 21, no.7, 1978, pp. 1100-1112.

[13]Hussain, A.K.M.F., and Zedan, M.G., "Effects of the Initial Condition on the Axisymmetric Free Shear Layer: Effect of the Initial Fluctuation Level," *Phys. Fluids*, Vol. 21, No. 9, 1978, pp. 1475-1481.

[14]Gutmark, E., Schadow, K.C., and Wilson, K.J., "Mixing Enhancement in coaxial Supersonic Jets," AIAA Paper 89-1812, 1989.

[15]Papamoschou, D., and Roshko, A., "The compressible turbulent mixing layer: an experimental study," *J.fluid Mech.*, Vol. 197, 1988, pp. 453-477.

[16]Samimy, M., and Elliot, G.S., "Effects of Compressibility on the characteristics of free shear layers," *AIAA J.*, vol. 28, 1990, pp. 439-445.

[17]Samimy, M., Reeder, M.F., and Elliott, G.S., "Compressibility effects on Large Structures in Free Shear Flows," *Phys. Fluids A*, Vol. 4, 1992, pp. 1251-1258.

[18]Marble, F.E., Zukoski, E.E., Jacobs, J.W., Hendricks, G.J., and Waitz, I.A., "Shock Enhancement and Control of Hypersonic Mixing and Combustion," AIAA Paper 90-1981, 1981.

[19]Budzinski, J.M., Zukoski, E.E., and Marble, F.E., "Rayleigh Scattering Measurements of Shock Enhanced Mixing," AIAA Paper 92-3546, 1992.

[20]Jacobs, J.W., "Shock-induced mixing of a light-gas cylinder," *J. Fluid Mech.*, Vol. 234, 1992, pp. 629-649.

[21]Gruber, M.R., and Nejad, A.S., "Development of a Large-Scale Supersonic Combustion Research Facility," AIAA Paper 94-0544, 1994.

[22]Miles, R. and Lempert W., "Two-Dimensional Measurement of Density, Velocity and Temperature in Turbulent High-Speed Air Flows by UV Rayleigh Scattering," *Appl. Phys. B*, Vol. 51, 1990, pp.1-7.

[23]Arnette, S.A., Samimy, M., and Elliot, G.S., "The Effect of Expansion on the Large Scale Structure of a Compressible Turbulent Boundary Layer," AIAA Paper 93-2991, 1993.

[24]Elliot, G.S., Samimy, M., and Arnette, S.A., "Filtered Rayleigh Scattering Based Measurements in Compressible Mixing Layers," AIAA Paper 92-3543, 1992.

[25]Clemens, N.T. and Mungal, M.G., "A Planar Mie Scattering Technique for Visualizing Supersonic Mixing Flows," *Exp. in Fluids*, Vol. 11, 1991, pp.175-185.

[26]Hermanson, J.C. and Winter M., "Imaging of a Transverse, Sonic Jet in Supersonic Flow," AIAA Paper 91-2269, 1991.

[27]Hermanson, J.C., and Winter M., "Mie Scattering Imaging of a Transverse, Sonic Jet in Supersonic Flow," *AIAA J.*, Vol. 31, No. 1, 1993, pp.129-132.

[28]Lozano, A., Yip, B., and Hanson, R.K., "Acetone: a Tracer for Concentration Measurements in Gaseous Flows by Planar Laser-Induced fluorescence," *Exp. in Fluids*, Vol. 13, 1992, pp. 369-376.

[29]Greenblatt, G.D., Ruhman, S., and Haas, Y., "Fluorescence Decay Kinetics of Acetone Vapor at Low Pressures," *Chem. Physics Letters*, Vol. 112, No. 3, 1984, pp. 200-206.

[30]Copeland, R.A., and Crosley, D.R., "Radiative, Collisional and Dissociative Processes in Triplet Acetone," *Chem. Physics Letters*, Vol. 115, No. 4,5, 1985, pp. 362-368.

[31]Balu, S., Donbar, J.M., and Nejad, A.S., "Numerical Study of Mixing in High and low Enthalpy Supersonic Test Facility", JANNAF Propulsion Meeting and 30th JANNAF Combustion Subcommittee Meeting, Moneterey, California, Nov. 1993.

[32]Gruber, M.R., Nejad, A.S., Chen, T., and Dutton, J. "Mixing and Penetration Studies of Sonic Jets in a Mach 2 Freestream," AIAA Paper 94-0709, 1994.

[33]Raffoul, C., and Nejad, A., Chen, T., and Dutton, J., "Entrainment and Mixing Characteristics of Bluff Body Flameholders; An Experimental and Numerical Study," AIAA Paper 94-0710, 1994.